

Charge transfer modification of inverted planar perovskite solar cells by NiO_x/Sr: NiO_x bilayer hole transport layer

Qiaopeng Cui(崔翘鹏), Liang Zhao(赵亮), Xuewen Sun(孙学文), Qiannan Yao(姚倩楠), Sheng Huang(黄胜), Lei Zhu(朱磊), Yulong Zhao(赵宇龙), Jian Song(宋健), and Yinghuai Qiang(强颖怀)

Citation: Chin. Phys. B, 2022, 31 (**3**): 038801. DOI: 10.1088/1674-1056/ac1fda
Journal homepage: http://cpb.iphy.ac.cn; http://iopscience.iop.org/cpb

What follows is a list of articles you may be interested in

Reveal the large open-circuit voltage deficit of all-inorganic $CsPbIBr_2$ perovskite solar cells

Ying Hu(胡颖), Jiaping Wang(王家平), Peng Zhao(赵鹏), Zhenhua Lin(林珍华), Siyu Zhang(张思玉),Jie Su(苏杰), Miao Zhang(张苗), Jincheng Zhang(张进成), Jingjing Chang(常晶晶), and Yue Hao(郝跃)
Chin. Phys. B, 2022, 31 (**3**): 038804. DOI: 10.1088/1674-1056/ac464b

High efficiency ETM-free perovskite cell composed of CuSCN and increasing gradient $CH_3NH_3PbI_3$

Tao Wang(汪涛), Gui-Jiang Xiao(肖贵将), Ren Sun(孙韧), Lin-Bao Luo(罗林保), and Mao-Xiang Yi(易茂祥)
Chin. Phys. B, 2022, 31 (**1**): 018801. DOI: 10.1088/1674-1056/ac0bb0

Non-peripherally octaalkyl-substituted nickel phthalocyanines used as non-dopant hole transport materials in perovskite solar cells

Fei Qi(齐飞), Bo Wu(吴波), Junyuan Xu(徐俊源), Qian Chen(陈潜), Haiquan Shan(单海权), Jiaju Xu(许家驹), and Zong-Xiang Xu(许宗祥)
Chin. Phys. B, 2021, 30 (**10**): 108801. DOI: 10.1088/1674-1056/ac1573

Stabilization of formamidinium lead iodide perovskite precursor solution for blade-coating efficient carbon electrode perovskite solar cells

Yu Zhan(占宇), Weijie Chen(陈炜杰), Fu Yang(杨甫), and Yaowen Li(李耀文)
Chin. Phys. B, 2021, 30 (**8**): 088803. DOI: 10.1088/1674-1056/abfbcb

Improved efficiency and stability of perovskite solar cells with molecular ameliorating of ZnO nanorod/perovskite interface and Mg-doping ZnO

Zhenyun Zhang(张振雲), Lei Xu(许磊), and Junjie Qi(齐俊杰)
Chin. Phys. B, 2021, 30 (**3**): 038801. DOI: 10.1088/1674-1056/abd748

Charge transfer modification of inverted planar perovskite solar cells by NiO_x/Sr:NiO_x bilayer hole transport layer

Qiaopeng Cui(崔翘鹏)[1], Liang Zhao(赵亮)[1], Xuewen Sun(孙学文)[1], Qiannan Yao(姚倩楠)[1], Sheng Huang(黄胜)[1,†], Lei Zhu(朱磊)[2], Yulong Zhao(赵宇龙)[1], Jian Song(宋健)[1,‡], and Yinghuai Qiang(强颖怀)[1]

[1] *The Jiangsu Province Engineering Laboratory of High Efficient Energy Storage Technology and Equipments, School of Materials Science and Physics, China University of Mining and Technology, Xuzhou* 221116, *China*

[2] *Advanced Analysis & Computation Center, China University of Mining and Technology, Xuzhou* 221116, *China*

(Received 16 July 2021; revised manuscript received 18 August 2021; accepted manuscript online 22 August 2021)

Perovskite solar cells (PSCs) are the most promising commercial photoelectric conversion technology in the future. The planar p–i–n structure cells have advantages in negligible hysteresis, low temperature preparation and excellent stability. However, for inverted planar PSCs, the non-radiative recombination at the interface is an important reason that impedes the charge transfer and improvement of power conversion efficiency. Having a homogeneous, compact, and energy-level-matched charge transport layer is the key to reducing non-radiative recombination. In our study, NiO_x/Sr:NiO_x bilayer hole transport layer (HTL) improves the holes transmission of NiO_x based HTL, reduces the recombination in the interface between perovskite and HTL layer and improves the device performance. The bilayer HTL enhances the hole transfer by forming a driving force of an electric field and further improves J_{sc}. As a result, the device has a power conversion efficiency of 18.44%, a short circuit current density of 22.81 mA·cm^{-2} and a fill factor of 0.80. Compared to the pristine PSCs, there are certain improvements of optical parameters. This method provides a new idea for the future design of novel hole transport layers and the development of high-performance solar cells.

Keywords: perovskite solar cells, nickel oxide, Sr doping, bilayer hole transport layer

PACS: 88.40.H–, 88.40.hj, 78.56.–a **DOI:** 10.1088/1674-1056/ac1fda

1. Introduction

Solar cells have attracted a great deal of attention, and the most glamorous star is organic-inorganic hybrid perovskite solar cells (PSCs) now. In recent years, researchers have concentrated on PSCs because of their rapid growth in power conversion efficiency (PCE).[1–5] So far, the PCE of PSCs has reached 25.2%,[6] their performance has almost caught up with currently commercialized silicon solar cells. Hybrid perovskite materials have many advantages, such as adjustable band gap, high absorption coefficient, long carrier life, and high carrier mobility.[7–10] Therefore, PSCs have potential to become the flagship of commercial solar power generation after silicon solar cells.[11] However, interface energy loss of different functional layers and alignment mismatch of energy levels still hinder performance enhancement of PSCs. Many scientists have made efforts in this regard.[12] Chen *et al.* reached a PCE of 19.35% by employing a NiO_x hole transport layer (HTL) with Cs.[13] Chen *et al.* suppressed the interfacial recombination by facile alkali chloride interface modification of the NiO_x HTL and obtained a device with PCE of 21%.[14] Zhu *et al.* used a larger alkylammonium interface layer to reduce the energy loss between the transport layer and the perovskite, and successfully achieved a inverted PSCs efficiency record of 22.3%.[15] Therefore, improving layer-to-layer interface is essential to promote the charge transfer process and to reduce carrier recombination so as to further improve the PCE.[16]

HTLs are designed to block electrons, enhance hole transport and prevent quenching caused by direct contact between the perovskite layer and conductive substrate in inverted PSCs. There are many HTLs based on polymers or small molecules, such as Spiro-OMeTAD, PEDOT:PSS, PTAA, and P3HT.[17] However, due to the natural instability of organic materials and relatively low work function, researchers are also actively studying inorganic hole transport materials. Inorganic p-type semiconductor materials, such as NiO, CuI, CuSCN, and graphene oxide are also taken as HTLs in inverted planar PSCs.[18–21] Among them, NiO_x has suitable work function, natural stability, and great energy level matching, which is widely used in the devices.[22,23]

However, NiO has a low intrinsic conductivity, which will cause holes to accumulate at the NiO_x/perovskite interface and to reduce hole extraction ability, so as to reduce the open circuit voltage (V_{oc}) and efficiency of devices.[24] Researchers are actively looking for strategies to improve the optical and electrical properties of NiO_x thin film. Doping can effectively improve conductivity of NiO_x films and adjust energy band position to well match with the energy levels. Dopants,

†Corresponding author. E-mail: huangsheng@cumt.edu.cn
‡Corresponding author. E-mail: jsoong@cumt.edu.cn

© 2022 Chinese Physical Society and IOP Publishing Ltd

such as Sr, Cu, Li, and Co[20,25–27] have been used to enhance charge transfer performance in NiO_x HTLs. However, doping not only greatly increases concentration of free carriers, but also brings lattice distortion and introduces new impurity levels, which will enlarge the possibility of carrier recombination. Therefore, doping is not always conducive to hole extraction at the interface of NiO_x and perovskite. Film surface modification[28–31] or various advanced film deposition methods[32–36] can be used to relieve charge recombination at charge transfer layer (CTL)/perovskite interface.

Our group previously proposed an ingenious strategy both to enhance the hole transport ability and to suppress charge recombination at CTL/perovsktie interfaces with a p–p^+ homojunction based on Cu doped NiO_x and Li doped NiO_x.[37,38] We found that other element doping such as Sr can also significantly increase the carrier concentration of NiO_x films. In this work, we further construct a NiO_x/Sr:NiO_x bilayer HTL to study its influence on interface carrier transport. We prepared an inverted planar PSC with a structure of FTO/Sr:NiO_x/NiO_x/perovskite/PCBM/BCP/Ag, showing an enhanced hole extraction ability and energy level matching because of the NiO_x/Sr:NiO_x bilayer HTL. In this device, Sr-doped NiO_x thin film has no direct contact with the perovskite layer. As a result, we obtain an improved PCE of 18.44% and a fill factor of 0.80 based on the bialyer HTL, which is much higher than that using Sr:NiO_x (16.89%) or NiO_x (15.69%).

2. Experiment

2.1. Preparation of the HTL

FTO glass (Nippon Sheet Glass) was first cut into a size of 19 mm×19 mm. The glasses was put in a glass washing rack, and washed by deionized water with dishwashing detergent, deionized water, ethanol, isopropanol, and ethanol in sequence, under ultrasonic for half an hour. Next, a precursor solution of nickel oxide was prepared, 0.727 g $Ni(NO_3)_2{\cdot}6H_2O$ was dissolved in 5 mL of ethylene glycol solution, and then 0.15 g ethylenediamine was added. For Sr doped NiO_x, additional 0.04233 g $Sr(NO_3)_2$ (Sr/Ni ratio in the precursor solution is 8%) was added. In order to eliminate the influence of film thickness, we used the same two-step spin coating method to prepare HTLs with three structures, including NiO_x, Sr:NiO_x, and NiO_x/Sr:NiO_x. The first layer was deposited by spin-coating under 5000 rpm for 30 s, after heating at 120 °C for 10 min, the second layer was deposited by the same procedure. Finally, the film was annealed at 400 °C for 1 h.

2.2. Fabrication of solar cell

A ternary cation mixed perovskite film using MA (methylammonium ion, $CH_3NH_3^+$), FA (formamidine ion, $HN{=}CHNH_3^+$) and Cs was prepared as the active layer. We took 0.0224 g MABr, 0.1719 g FAI, 0.5071 g PbI_2, and 0.0734 g $PbBr_2$ and dissolved them in a mixed solvent (1 mL) with a volume ratio of DMSO and DMF of 1:4. After two hours of thorough mixing, 84 μL of CsI (1.5 mol/L, DMSO as solvent) was added. The final formula ratio of perovskite is $Cs_{0.1}(MA_{0.12}FA_{0.88})_{0.9}Pb(I_{0.95}Br_{0.05})_3$. Then 60 μL of filtered perovskite precursor solution was dropped on the prepared HTL film, spinning at 1000 rpm for 10 s, and then sped to 4000 rpm. After 8 s, 200 μL of ethyl acetate was quickly dropped. The obtained perovskite film was then heated at 70 °C for 3 min, and 100 °C for 10 min. Next, 45 μL of PCBM (25 mg/mL, chlorobenzene as solvent) was spin-coated at 3000 rmp for 30 s to prepare the electron transport layer. Subsequently, 45 μL of BCP (0.5 mg/mL, ethanol as solvent) was deposited on PCBM at 3000 rpm for 30 s. Finally, a vacuum thermal evaporation method was used to deposit 50 nm silver to form metal electrode.

2.3. Characterization

We used x-ray diffraction (XRD, D8 Advance, Bruker), energy-dispersive x-ray spectroscopy (EDS, XFlash QUAD SVE6, Burker), x-ray photoelectron spectra (XPS, ESCALAB250Xi, Thermo Fisher), field emission scanning electron microscope (FESEM, SU8220, Hitachi) to observe the crystal structure, element composition and distribution, film morphology of NiO_x-based HTLs and perovskite films. UV-visible (UV-Vis spectrophotometer, Cary 300, Varian) was used to test optical property of HTLs. The Hall effect measurement (ezHEMS, NanoMagnetics) was used to demonstrate the carrier properties of HTL. For the Fermi level and valence-band edge of NiO_x and Sr:NiO_x films, we used an ultraviolet photoelectron spectroscope (UPS, Thermo Fisher) with a monochromatic He light source (21.21 eV) to calculate them. Steady state photoluminescence spectra (PL, FS5, Edinburgh) and transient time-resolved photoluminescence (TRPL, FLS980, Edinburgh) were recorded by spectrofluorometer. Electrochemical workstation (Keithley 2420 Source Meter) was selected to measure the photocurrent–voltage (J–V) curves of inverted planar PSCs under solar illumination (100 $mW{\cdot}cm^{-2}$, Oriel Sol 3 A, Newport) with 10 mV voltage steps and dwell time of 50 ms. The PSCs were tested with an active area of 0.05 cm^2. The light intensity was calibrated by a standard Si-cell (Oriel Instrument). HTL conductivity was evaluated by I–V curves of NiO_x films directly vaporized by silver at the same electrochemical workstation. The dark I–V curves (SCLC) were noted from 0 V to 3 V with 10 mV steps and dwell time of 10 ms (Keithley 2420 Source Meter). We used a power source (Newport 300W Xenon lamp, 66902) with a monochromator (Newport Cornerstone 260) and a power meter (Newport 2936-C) to measure

incident photon to current conversion efficiency (IPCE). Electrochemical impedance spectroscopy (EIS, CHI660E, CH Instruments) was recorded under dark condition at a bias voltage of 0.6 V from 100 kHz to 1 Hz with amplitude of 5 mV and quiet time of 2 s.

3. Results and discussion

As shown in Fig. S1, the XRD results of NiO_x films with or without Sr doping indicate that doping process does not change crystal phase of NiO_x, nor does it produce other Sr-containing compounds. We find that Sr are evenly distributed in the NiO_x film, as shown in Fig. 1(a). Additionally, Sr-doping does not evidently change the morphology of NiO_x-based films (Fig. 1(b) and Fig. S2), they all present a dense morphology with some nanoparticles aggregation on the surface, which is beneficial for deposition of the perovksite layer. The similar morphology of NiO_x substrates lead to indistinguishable phase structure difference of the deposited perovksite films (Fig. S1b). The cross-sectional SEM image in Fig. 1(b) clearly shows all the functional layers of the devices. XPS test was used to prove the valence state of Ni and the doping state of Sr. In XPS survey of Sr:NiO_x, we can find a characteristic peak of Sr (Fig. S3), which proves the successful incorporation of Sr in the NiO_x film. In addition to the characteristic peaks of Sr, Ni, O, the width scans spectrum also show characteristic peaks of Na and Si, due to the special composition of FTO glass. As shown in Figs. 1(c) and 1(d), two different oxidation states of Ni^{2+} and Ni^{3+} can be well represented by the Gaussian function fitting the spectrum of Ni 2p 3/2. The main peak at 852.89 eV and the shoulder peak at 854.7 eV correspond to Ni^{2+} and Ni^{3+}, respectively.[39,40] The ratio of simulated peak area of Ni^{3+} to Ni^{2+} is 1.21, which is significantly higher than that of pure NiO_x film (1.01), the higher ratio of Ni^{3+} to Ni^{2+} indicates a larger hole concentration in the film.[41] This result is further demonstrated by the Hall-effect measurement, as shown in Table S1, both NiO_x and Sr:NiO_x films have p-type property, and the doped film has a much higher charge mobility and carrier density.[42] The *I–V* curves of different HTLs also manifest the advantages of doping process in the improvement of film electroconductivity (Fig. S4).[43]

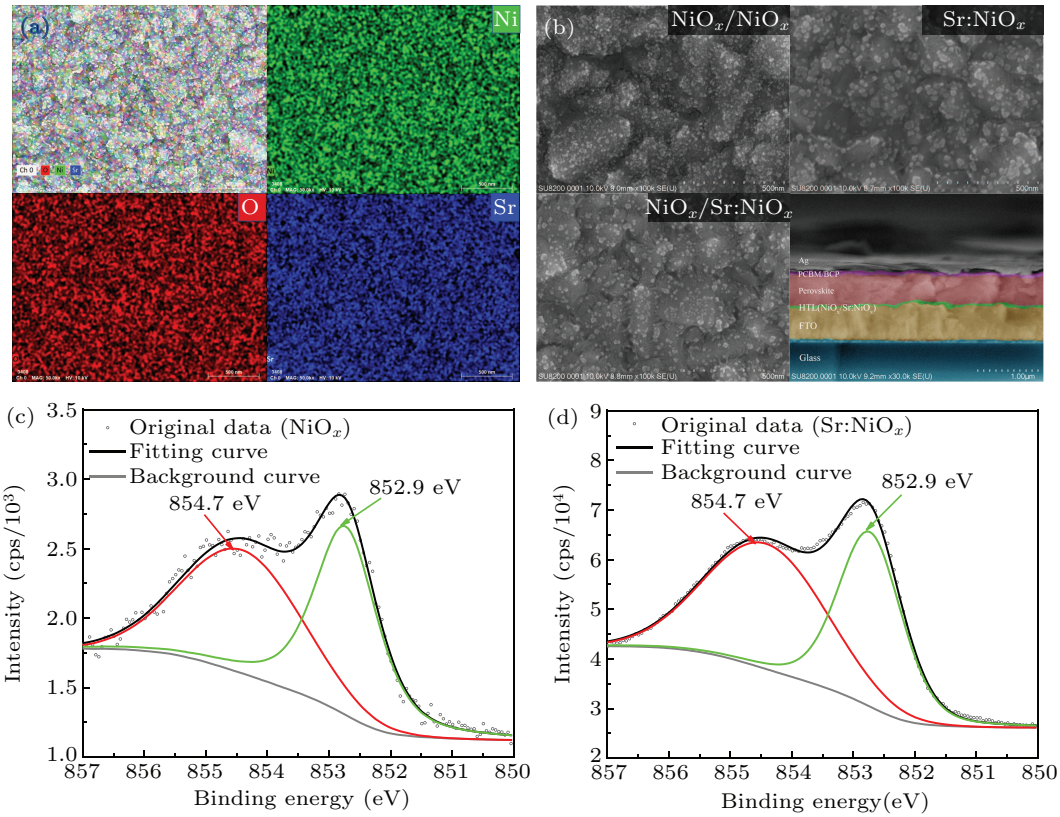


Fig. 1. (a) EDS-mapping spectrum of O, Ni, Sr in Sr:NiO_x film. (b) SEM images of NiO_x, Sr:NiO_x and NiO_x/Sr:NiO_x films, and SEM cross-section image of the device. XPS spectrum of Ni in (c) NiO_x and (d) Sr:NiO_x films.

Energy level alignment of NiO_x, Sr:NiO_x, and perovskite film (PVSK) is important for the analysis of carrier transport from the perovskite active layer to the HTL, so we first used the UV-vis absorption spectra and the UPS (Figs. S5 and S6) to measure the energy level structure of all the functional layers. Through UV-vis measurement, we found that the absorbance of Sr:NiO_x and pure NiO_x HTL are similar (Fig. S5a), and the calculated band gaps (E_g) are also very close to each other (Fig. S5b). This means that Sr doping does not change light absorbance of the NiO_x HTL. Figure S6 shows cut-off energy

and valence band edge in NiO_x, Sr:NiO_x and perovskite thin-film by UPS measurements, we can further calculate the Fermi level and valence band maximum (VBM) of semiconductors. The work function is the difference between the Fermi level and the vacuum level, so the work function is defined as $\phi = 21.21 - E_{\text{cutoff}}$.[44] According to the formula, ϕ of NiO_x is 5.15 eV, ϕ of Sr:NiO_x is 5.21 eV, and ϕ of PVSK is 5.12 eV. The valence band edge is the difference between the Fermi level and the VBM value, so the VBM values of NiO_x, Sr:NiO_x and perovskite film are −6.00 eV, −6.02 eV, and −6.36 eV, respectively. The energy level structure of hole transport layers and perovskite calculated from the relevant test results is shown in Fig. 2(a). The results indicate that the Fermi energy level decreases with Sr doping. This is consistent with the semiconductor doping law and previously report.[20] We also notice that the Fermi energy level of NiO_x is 0.06 eV higher than Sr:NiO_x, after contacting of these two films, band bending at the interface will happen and the bending direction is shown in Fig. 2(b), which is helpful for transportation of holes. Moreover, based on the same band bending rules, the photogenerated holes in the perovskite films could also be effectively extracted by the NiO_x film. Compared to the single layer HTL, the NiO_x/Sr:NiO_x bilayer HTL could produce an additional driving force for hole transport, which may accelerate carrier transport and inhibit interface recombination at HTL/PVSK.

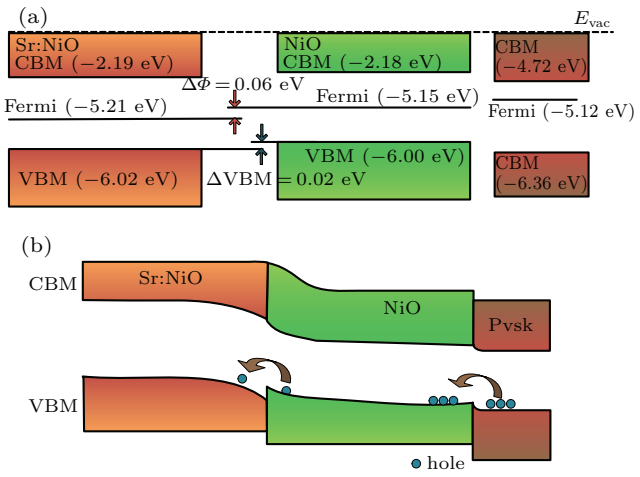


Fig. 2. Energy level structure of HTLs and perovskite film (a) before and (b) after contacting, and the transport of photogenerated holes in different films.

The *J*–*V* curves of PSCs based on different HTLs are presented in Fig. 3, and the corresponding photovoltaic parameters are listed in Table 1. The device using the NiO_x/Sr:NiO_x bilayer HTL shows the best performance, exhibiting a PCE of 18.44%, a V_{oc} of 1.01 V, a short circuit current density (J_{sc}) of 22.81 mA·cm^{-2}, and a fill factor (FF) of 0.80. Compared to the devices employing single layer HTLs, the device based on the bilayer HTL has evident advantages in all photovoltaic parameters. The result demonstrates that the bilayer HTL could realize our expectations that proper design of energy level alignment in HTL is useful to improve charge transfer and to decrease carrier recombination. Under the driving force of electric field generated in the bilayer HTL, the hole transport efficiency could be greatly improved. Additionally, we find that the device based on the single-layer Sr-doped NiO_x HTL could enhance the performance compared to the one using the NiO_x HTL, especially on the parameters of J_{sc} and FF because of the better conductivity of the doped film. However, its V_{oc} does not increase obviously, which should be ascribed to some additional defects in the Sr:NiO_x film introduced by the doping process, these defects would play as carrier recombination sites at HTL/perovskite interface. In regard to the NiO_x/Sr:NiO_x bilayer HTL, the doped film does not directly contact with the perovskite layer, so no additional defects are introduced to the interface. In Fig. 3(a), all the three devices have negligible hysteresis, presenting the advantage of inverted PSCs. The IPCE and integrated J_{sc} are shown in Fig. 3(b), the integrated J_{sc} data are close to the values shown in the *J*–*V* curves. Figures 3(c) and S7 show the statistic results of PCE, J_{sc}, V_{oc}, and FF, respectively. We find that the bilayer HTL presents apparent advantage in PCE, J_{sc}, and FF with higher average values and narrow distribution, compared to the other two HTLs. Figure 3(d) shows the great working stability of the best performance PSC using NiO_x/Sr:NiO_x HTL without encapsulation, the PCE maintains 89% after 192 h. The effect of Sr concentration in the NiO_x/Sr:NiO_x bilayer HTL has been investigated, as shown in Fig. S8 and Table S2. The ratio for Sr/Ni is closely related to device performance. As the Sr/Ni increases from 0 to 8%, photovoltaic performance enhances apparently because of the improved electrical property of the Sr:NiO_x film. However, as the ratio of Sr/Ni reaches 10%, the device performance decreases slightly, which may be induced by the lattice disorder as the over-doping process.

Table 1. Photovoltaic parameters of the champion inverted planar PSCs based on different HTLs.

HTL	Scan direction	J_{sc} (mA·cm^{-2})	V_{oc} (V)	FF	PCE (%)
NiO_x	Forward	20.69	0.97	0.78	15.69
	Reverse	20.86	1.01	0.73	15.51
Sr:NiO_x	Forward	21.98	0.97	0.79	16.89
	Reverse	21.54	0.99	0.78	16.64
NiO_x/Sr:NiO_x	Forward	22.81	1.01	0.80	18.44
	Reverse	23.02	1.00	0.79	18.31

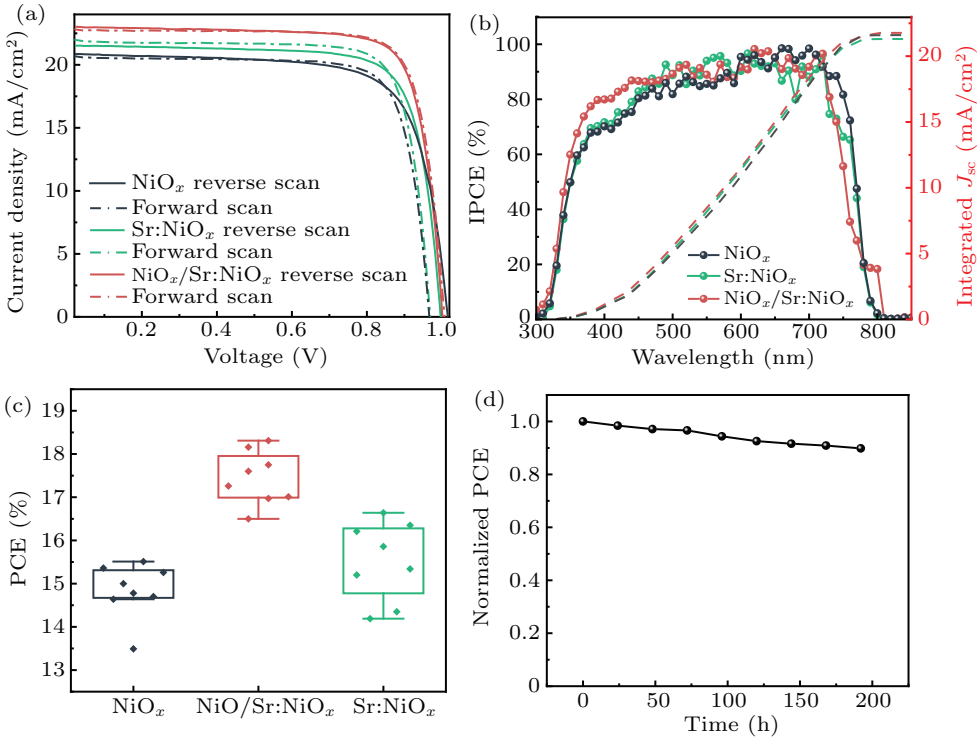


Fig. 3. (a) The *J*–*V* curves of champion PSCs based on different HTLs under reverse and forward scans. (b) IPCE spectrum and integrated J_{sc}. (c) Statistic results of PCE of the devices based on varied HTLs. (d) Normalized PCE as a function of time (hour) for best performance PSC using the NiO_x/Sr:NiO_x HTL without encapsulation.

In order to understand carrier dynamics at interfaces, the film was tested by steady-state photoluminescence (PL). We prepared the samples with the structure of FTO/HTL/PVSK, using the same preparation method as the solar cells. We find that the emission peak of the Sr:NiO_x-based film has an overall decrease compared to the emission peak of NiO_x-based one, as shown in Fig. 3(a). This decrease may be induced by the better carrier extraction of Sr:NiO_x from the perovskite film as its enhanced conductivity, but it could also originate from the increased non-radiative carrier recombination as the introduction of additional defects in the Sr:NiO_x film. However, the emission peak decrease of the NiO_x/Sr:NiO_x-based film should be induced by the enhanced charge transport and inhibits carrier recombination at the HTL/perovskite interface, because it is NiO_x but not Sr:NiO_x that directly contacts with the perovskite film.[45] Time-resolved photoluminescence spectroscopy (TRPL) is further used to study the charge carrier transport, the curves in Fig. 4(b) can be fitted with the equation

$$n(t) = A_1 \exp(-t/\tau_1) + A_2 \exp(-t/\tau_2), \quad (1)$$

where τ_1 and τ_2 are the life parameters of fast decay and slow decay, respectively. The fast decay process should be attributed to charge transfer at HTL/perovskite interface, and the slow decay should be ascribed to bimolecular radiative recombination.[46] We summarized the life parameters of the devices based on varied HTLs in Table 2. For comparison of τ_1, we know that the value of NiO_x/Sr:NiO_x-based film is the shortest. A short τ_1 value represents effective hole extraction at the HTL/PVSK layer.[47] In addition, the values of τ_2 are all above 400 ns, indicating the low level of defects in perovskite films and a slow carrier radiative recombination velocity.

Table 2. Parameters of the TRPL lifetime from fitting curves of the measurements.

HTL	A_1 (%)	τ_1 (ns)	A_2 (%)	τ_2 (ns)
NiO_x	1.05	14.41	98.95	562.29
Sr:NiO_x	0.95	3.53	99.05	549.33
NiO_x/Sr:NiO_x	2.92	1.96	97.08	428.41

In order to determine the effect of Sr doping on the density of defect states in NiO_x films, a dark current–voltage (*I*–*V*) test was performed using the space charge limited current (SCLC) model, as shown in Fig. 4(c). We can see that the first half of the linear relationship is in the ohmic region. When the applied voltage exceeds a certain value, the current increases rapidly. The value of the inflection point is named as the trap filled limit voltage (V_{TFL}).[48] Obviously, V_{TFL} of the NiO_x/Sr:NiO_x film is 0.735 V, which is lower than those of both NiO_x and Sr:NiO_x, indicating a lower density of defect states. The low V_{TFL} originates from the improved charge transfer process at HTL/perovskite interface. Moreover, the recombination mechanism is further studied by measuring the ideal factor associated with a specific recombination characteristic as a function of V_{oc}. Figure 4(d) shows the dependence of light intensity on V_{oc}. The curve is approximately fitted as a linear function curve. The ideal factors of the devices based on NiO_x, Sr:NiO_x, and NiO_x/Sr:NiO_x are 1.64,

1.48, and 1.31, respectively. The ideality factor closer to 1 indicates a lower single-molecule Shockley–Read–Hall (SRH) recombination. This result is consistent with the increased FF values by introducing the bilayer HTL, induced by the enhanced charge extraction and decreased carrier recombination at HTL/perovskite interface.[49] Furthermore, EIS delivers carriers transferring and recombination behaviors, as shown in Fig. 4(e). Parameters fitted are summarized in Table S3. The transport resistance R_{tr}, series resistance R_s, and the recombination resistance R_{rec} at the interface of PVSK/HTLs are displayed.[47] It can be observed clearly that R_{rec} of the NiO_x/Sr:NiO_x based device increases to 77428 Ω, which is much higher than the others. Compared with the control device, R_s and R_{tr} do not change significantly based on different HTLs. This indicates that NiO_x/Sr:NiO_x homojunction HTL devices restrain the recombination at the interface and accelerate the transfer of charge carriers,[48] EIS results are in accordance with the other measurements stated above.

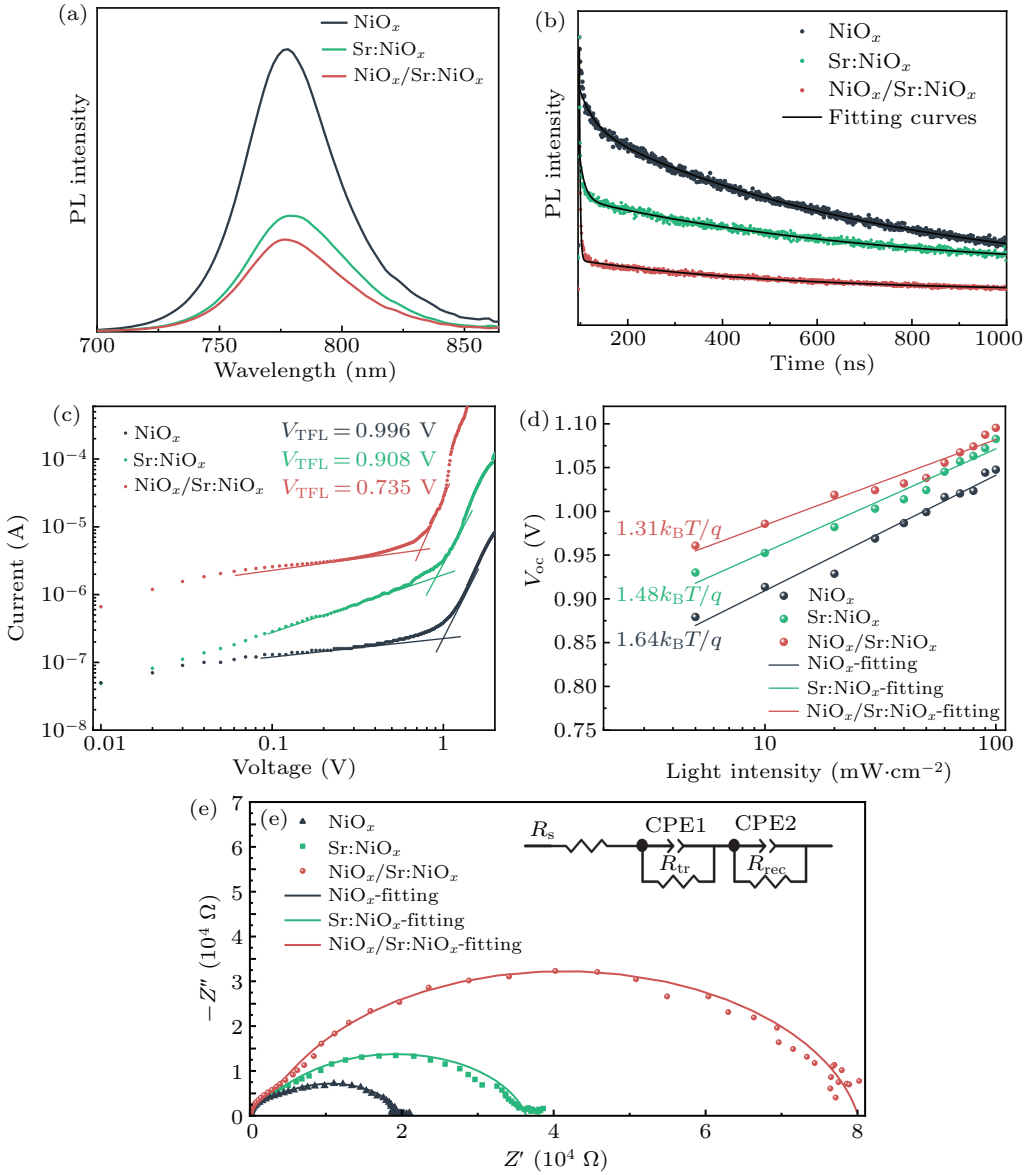


Fig. 4. (a) Steady-state photoluminescence (PL) spectra, and (b) transient time-resolved photoluminescence spectrum of FTO/HTL/perovskite. (c) Dark *I*–*V* curves of the HTL-only devices. (d) Light intensity dependent V_{oc} for inverted planar PSCs based on different HTLs. (e) Nyquist plots of devices based on different HTLs under a bias of 0.6 V.

4. Conclusion

The bilayer hole transport layer we constructed for inverted planar PSC is composed of NiO_x/Sr:NiO_x. Sr doping significantly increases the ratio of Ni^{3+}/Ni^{2+} in the Sr:NiO_x film, thereby increasing its charge transfer property. The Fermi level of Sr:NiO_x decreases compared to NiO_x and the band direction after contacting with NiO_x could produce a driving force for holes extracting and reduce the recombination at the interface between the perovskite and HTL layers. Based on this bilayer strategy, we obtain an inverted planar PSC with PCE of 18.44%, J_{sc} of 22.81 mA·cm^{-2} and FF of 0.80, higher than the ones using NiO_x or Sr:NiO_x. This strategy provides a new idea for the future design of novel hole

transport layers, which is effective to make high performance solar cells.

Acknowledgement

This work was supported by the Fundamental Research Funds for the Central Universities, China (Grant No. 2021QN1110).

References

[1] Kojima A, Teshima K, Shirai Y and Miyasaka T 2009 *J. Am. Chem. Soc.* **131** 6050
[2] Arora N, Dar M I, Hinderhofer A, Pellet N, Schreiber F, Zakeeruddin S M and Grätzel M 2017 *Science* **358** 768
[3] Wang L, Zhou H, Hu J, Huang B, Sun M, Dong B, Zheng G, Huang Y, Chen Y, Li L, Xu Z, Li N, Liu Z, Chen Q, Sun L D and Yan C H 2019 *Science* **363** 265
[4] Wang Y, Wu T, Barbaud J, Kong W, Cui D, Chen H, Yang X and Han L 2019 *Science* **365** 687
[5] Song J, Li S P, Zhao Y L, Yuan J, Zhu Y, Fang Y, Zhu L, Gu X Q and Qiang Y H 2017 *J. Alloys Compd.* **694** 1232
[6] Jeong J, Kim M, Seo J, Lu H, Ahlawat P, Mishra A, Yang Y, Hope M A, Eickemeyer F T, Kim M, Yoon Y J, Choi I W, Darwich B P, Choi S J, Jo Y, Lee J H, Walker B, Zakeeruddin S M, Emsley L, Rothlisberger U, Hagfeldt A, Kim D S, Grätzel M and Kim J Y 2021 *Nature* **592** 381
[7] Jeon N J, Noh J H, Yang W S, Kim Y C, Ryu S, Seo J and Seok S I 2015 *Nature* **517** 476
[8] Yuan S, Liu Q W, Tian Q S, Jin Y, Wang Z K and Liao L S 2020 *Adv. Funct. Mater.* **30** 1909222
[9] Lee M M, Teuscher J, Miyasaka T, Murakami T N and Snaith H J 2012 *Science* **338** 643
[10] Wehrenfennig C, Eperon G E, Johnston M B, Snaith H J and Herz L M 2014 *Adv. Mater.* **26** 1584
[11] Yang Y, Song J, Zhao Y L, Zhu L, Gu X Q, Gu Y Q, Che M and Qiang Y H 2016 *J. Alloys Compd.* **684** 84
[12] Xi J, Xi K, Sadhanala A, Zhang K H L, Li G, Dong H, Lei T, Yuan F, Ran C, Jiao B, Coxon P R, Harris C J, Hou X, Kumar R V and Wu Z 2019 *Nano Energy* **56** 741
[13] Chen W, Liu F Z, Feng X Y, Djurišić A B, Chan W K and He Z B 2017 *Adv. Energy Mater.* **7** 1700722
[14] Chen W, Zhou Y, Chen G, Wu Y, Tu B, Liu F Z, Huang L, Ng A M C, Djurišić A B and He Z 2019 *Adv. Energy Mater.* **9** 1803872
[15] Wu S, Zhang J, Li Z, Liu D, Qin M, Cheung S H, Lu X, Lei D, So S K, Zhu Z and Jen A K Y 2020 *Joule* **4** 1248
[16] Song J, Yang Y, Zhao Y L, Che M, Zhu L, Gu X Q and Qiang Y H 2017 *Mater. Sci. Engin. B* **217** 18
[17] Malinkiewicz O, Yella A, Lee Y H, Espallargas G M, Graetzel M, Nazeeruddin M K and Bolink H J 2014 *Nat. Photon.* **8** 128
[18] Hou S, Shi B, Wang P, Li Y, Zhang J, Chen P, Chen B, Hou F, Huang Q, Ding Y, Li Y, Zhang D, Xu S, Zhao Y and Zhang X 2020 *Chin. Phys. B* **29** 078801
[19] Chen W Y, Deng L L, Dai S M, Wang X, Tian C B, Zhan X X, Xie S Y, Huang R B and Zheng L S 2015 *J. Mater. Chem. A* **3** 19353
[20] Chen W, Wu Y, Fan J, Djurišić A B, Liu F, Tam H W, Ng A, Surya C, Chan W K, Wang D and He Z B 2018 *Adv. Energy Mater.* **8** 1703519
[21] Liu T, Chen K, Hu Q, Zhu R and Gong Q 2016 *Adv. Energy Mater.* **6** 1600457
[22] Qiu Q, Mou J, Song J and Qiang Y 2020 *J. Electron. Mater.* **49** 6300
[23] Liu H, Song J, Qin Y, Mou J, Qiu Q, Zhao Y, Zhu L and Qiang Y 2020 *Vacuum* **172** 109077
[24] Corani A, Li M H, Shen P S, Chen P, Guo T F, El Nahhas A, Zheng K, Yartsev A, Sundström V and Ponseca C S 2016 *J. Phys. Chem. Lett.* **7** 1096
[25] Zhang J, Mao W, Hou X, Duan J, Zhou J, Huang S, Ou-Yang W, Zhang X, Sun Z and Chen X 2018 *Solar Energy* **174** 1133
[26] Park M A, Park I J, Park S, Kim J, Jo W, Son H J and Kim J Y 2018 *Curr. Appl. Phys.* **18** S55
[27] Xie Y, Lu K, Duan J, Jiang Y, Hu L, Liu T, Zhou Y and Hu B 2018 *ACS Appl. Mater. Interfaces* **10** 14153
[28] Li Z, Jo B H, Hwang S J, Kim T H, Somasundaram S, Kamaraj E, Bang J, Ahn T K, Park S and Park H J 2019 *Adv. Sci.* **6** 1802163
[29] Zhang B, Su J, Guo X, Zhou L, Lin Z, Feng L, Zhang J, Chang J and Hao Y 2020 *Adv. Sci.* **7** 1903044
[30] Qiu Q, Liu H, Qin Y, Ren C and Song J 2020 *J. Mater. Sci.* **55** 13881
[31] Yang F, Wang C, Pan Y, Zhou X, Kong X and Ji W 2019 *Chin. Phys. B* **28** 056402
[32] Wang S F, Shi L Y, Feng X and Ma S R 2007 *Mater. Lett.* **61** 1549
[33] Zhu Z, Bai Y, Zhang T, Liu Z, Long X, Wei Z, Wang Z, Zhang L, Wang J and Yan F 2014 *Angew. Chem.* **126** 12779
[34] Liu Y, Song J, Qin Y, Qiu Q, Zhao Y, Zhu L and Qiang Y 2019 *J. Mater. Sci.: Mater. Electron.* **30** 15627
[35] Sui G, Li J, Du L, Zhuang Y, Zhang Y, Zou Y and Li B 2020 *J. Alloys Compd.* **823** 153851
[36] Liu D, Li D and Yang D 2016 *Cryst. Res. Technol.* **51** 313
[37] Song J, Zhao L, Huang S, Yan X, Qiu Q, Zhao Y, Zhu L, Qiang Y, Li H and Li G 2021 *ChemSusChem* **14** 1396
[38] Zhao L, Sun X, Yao Q, Huang S, Zhu L, Song J, Zhao Y and Qiang Y 2022 *Adv. Mater. Interfaces* **9** 2101562
[39] Chen W, Wu Y, Yue Y, Liu J, Zhang W, Yang X, Chen H, Bi E, Ashraful I and Grätzel M 2015 *Science* **350** 944
[40] Martin L, Martinez H, Poinot D, Pecquenard B and Le Cras F 2013 *J. Phys. Chem. C* **117** 4421
[41] Zhang K H, Xi K, Blamire M G and Egdell R G 2016 *J. Phys.: Condens. Matter* **28** 383002
[42] Gu Y F, Du H J, Li N N, Yang L and Zhou C Y 2019 *Chin. Phys. B* **28** 048802
[43] Zheng J, Hu L, Yun J S, Zhang M, Lau C F J, Bing J, Deng X, Ma Q, Cho Y, Fu W, Chen C, Green M A, Huang S and Ho-Baillie A W Y 2018 *ACS Appl. Energy Mater.* **1** 561
[44] Chen W Y, Deng L L, Dai S M, Wang X, Tian C B, Zhan X X, Xie S Y, Huang R B and Zheng L S 2015 *J. Mater. Chem. A* **3** 19353
[45] Chandrasekhar P, Dubey A and Qiao Q 2020 *Solar Energy* **197** 78
[46] Kanaya S, Kim G M, Ikegami M, Miyasaka T, Suzuki K, Miyazawa Y, Toyota H, Osonoe K, Yamamoto T and Hirose K 2019 *J. Phys. Chem. Lett.* **10** 6990
[47] Jeon N J, Na H, Jung E H, Yang T Y, Lee Y G, Kim G, Shin H W, Seok S I, Lee J and Seo J 2018 *Nat. Energy* **3** 682
[48] Lv Y, Cai B, Ma Q, Wang Z, Liu J J and Zhang W H 2018 *RSC Adv.* **8** 20982
[49] Caprioglio P, Stolterfoht M, Wolff C M, Unold T, Rech B, Albrecht S and Neher D 2019 *Adv. Energy Mater.* **9** 1901631